

Spaxel Analysis: Probing the Physics of Star Formation in Ultraluminous Infrared Galaxies

Michael A. Dopita¹²³, Jeffrey Rich⁴, Frédéric P. A. Vogt¹, Lisa J. Kewley¹³, I-Ting Ho³, Hassan M. Basurah², Alaa Ali² & Morsi A. Amer²

Abstract This paper presents a detailed spectral pixel (spaxel) analysis of the ten Luminous Infrared Galaxies (LIRGs) previously observed with the Wide Field Spectrograph (WiFeS), an integral field spectrograph mounted on the ANU 2.3m telescope, and for which an abundance gradient analysis has already been presented by Rich et al. (2012). Here we use the strong emission line analysis techniques developed by Dopita et al. (2013) to measure the ionisation parameter and the oxygen abundance in each spaxel. In addition, we use the observed H α flux to determine the surface rate of star formation ($M_{\odot}\text{yr}^{-1}\text{kpc}^{-2}$) and use the [S II] $\lambda\lambda 6717/6731$ ratio to estimate the local pressure in the ionised plasma. We discuss the correlations discovered between these physical quantities, and use them to infer aspects of the physics of star formation in these extreme star forming environments. In particular, we find a correlation between the star formation rate and the inferred ionisation parameter. We examine the possible reasons for this correlation, and determine that the most likely explanation is that the more active star forming regions have a different distribution of molecular gas which favour higher ionisation parameters in the ionised plasma.

Michael A. Dopita, Jeffrey Rich, Frédéric P. A. Vogt, Lisa J. Kewley, I-Ting Ho, Hassan M. Basurah, Alaa Ali & Morsi A. Amer

¹Research School of Astronomy and Astrophysics, Australian National University, Cotter Rd., Weston ACT 2611, Australia

²Astronomy Department, King Abdulaziz University, P.O. Box 80203, Jeddah, Saudi Arabia

³Institute for Astronomy, University of Hawaii, 2680 Woodlawn Drive, Honolulu, HI 96822, USA

⁴Carnegie Observatories, 813 Santa Barbara Street, Pasadena, CA 91101, USA

1 Introduction

The Ultraluminous Infrared Galaxies (ULIRGs) provide a vital link between star formation processes occurring in the local universe, and star formation in high redshift galaxies. Although rather rare in the local Universe, ULIRGs account for a much greater fraction of star formation by $z \sim 1$ when encounters between galaxies was much more frequent (Le Floch et al. 2005; Magnelli et al. 2011). By the study of ULIRGs, we hope to understand the physics triggering star formation in merging systems, and to discover whether, for example, the initial mass function (IMF) is biased towards more massive stars (Hoversten, & Glazebrook 2008; van Dokkum 2008; Meurer et al. 2009; Treu et al. 2010; Cappellari et al. 2012; Andrews et al. 2013; Bekki & Meurer 2013), or discover whether the mass distribution of stellar clusters themselves is somehow different in regions of very high star formation rates (Portegies et al. 2010; Chandar et al. 2010; Adamo et al. 2010; Weidner, Kroupa & Pflamm-Altenburg 2011). Although these issues have been studied through surface photometry, the advent of integral field spectrographs is relatively recent, and the use of these to simultaneously measure the relationship of star formation, metallicity, gas pressure and the excitation of the H II regions surrounding the newly formed star clusters is only in its infancy.

In this paper, we investigate the utility of spaxel (spectral pixel) analysis for the study of local ULIRGs which are not dominated by shock-excited gas such as those described by Rich, Kewley & Dopita (2011). The targets are ULIRGs drawn from the Great Observatory All-Sky LIRG Survey (GOALS) sample (Armus et al. 2009). GOALS is a multi-wavelength survey of the brightest $60\mu\text{m}$ extragalactic sources in the local universe ($\log(L_{\text{IR}}/L_{\odot}) > 11.0$) and with redshifts $z < 0.088$. The GOALS sample is a complete subset of the IRAS Revised Bright Galaxy Sample (RBGS)

(Sanders et al. 2003). Objects in GOALS cover the full range of nuclear spectral types and interaction stages and, given their luminosity distribution, serve as useful analogs for comparison with high-redshift galaxies.

2 Observations

The galaxies analysed here are the same as those analysed by Rich et al. (2012) for the derivation of the abundance gradients and reddening. We refer the reader to that paper for the spatial orientations, reddening maps and other global properties of these galaxies. All of the galaxies lie in the restricted luminosity range $11.93 > \log(L_{\text{IR}}/L_{\odot}) > 11.41$. Table 1 gives the names, the adopted luminosity distances and the IR luminosities of the target objects.

All observations were made with the Wide Field Field Spectrograph (WiFeS) located at the Mount Stromlo and Siding Spring Observatory 2.3m telescope. This dual-beam image-slicing integral field spectrograph is described by Dopita et al. (2007), and its on-telescope performance is described in Dopita et al. (2010a). It provides a 25×38 arc sec. field of view with the 1.0 arc sec. square spaxels fully filling the field. Our observations used the R7000 and B3000 gratings giving a 5700-7000Å spectral range in the red at a resolution of $R \sim 7000$ (FWHM = 40 km s⁻¹) and spectral coverage of 3700-5700Å at a resolution of $R \sim 3000$ (FWHM = 100 km s⁻¹) in the blue. The data reduction and analysis procedures are fully described in earlier papers (Rich et al. 2010; Rich, Kewley & Dopita 2011; Rich et al. 2012) and will not be repeated here.

Table 1 The GOALS galaxies analysed in this paper.

(1) IRAS No.	(2) Other Name	(3) Distance (Mpc)	(4) $\log(L_{\text{IR}}/L_{\odot})$
F01053-1746	IC 1623 A/B	82.3	11.71
IRAS 08355-4944	–	112	11.62
F10038-3338	ESO 374-IG032	145.8	11.78
F10257-4339	NGC 3256	38.2	11.64
F13373+0105 E/W	Arp 240	103.5	11.62
F17222-5953	ESO 138-G027	94	11.41
F18093-5744 N/S	IC 4687/4689	79/82	11.62
F18341-5732	IC 4734	70.9	11.35
F19115-2124	ESO 593-IG008	201	11.93

3 The Spaxel Analysis

In our analysis we seek to attach to each spectral pixel (spaxel) a star formation rate, a gas pressure, P/k , an oxygen abundance, $12 + \log(\text{O}/\text{H})$, and an ionisation parameter q (related to the dimensionless ionisation parameter $\mathcal{U} = q/c$, where c is the speed of light). For each spaxel, de-reddened emission line fluxes were derived for all the strong lines from the [O II] doublet $\lambda\lambda 3726, 29$ all the way up to the [S II] doublet $\lambda\lambda 6717, 31$.

The star formation is derived from the H α flux. This is possible because flux in a hydrogen line is proportional to the number of photons produced by the hot stars, which is in turn proportional to their birthrate. This relationship was earlier calibrated by Dopita & Ryder (1994). Here we use the “standard” calibration for starbursts by Kennicutt (1998), based on the Starburst 99 models of Leitherer & Heckman (1995):

$$SFR_{\text{H}\alpha} = 7.9 \times 10^{-42} [L_{\text{H}\alpha}/\text{erg.s}^{-1}] \quad (1)$$

Using the surface brightness per square arc sec. and the distance we can translate this star formation rate to the (local) surface rate of star formation in units of $\text{M}_{\odot}\text{yr}^{-1}\text{kpc}^{-2}$.

The mean gas pressure in the ionised plasma is derived from the [S II] $\lambda\lambda 6731/6717$ ratio. This line ratio is almost insensitive to electron density below $n_e \sim 50 \text{ cm}^{-3}$, so in effect pressures of $\log(P/k) < 5.5 \text{ Kcm}^{-3}$ cannot be measured. Since most of the galaxies measured here have super-solar metallicities, their electron temperatures are low; $T_e \lesssim 5000 \text{ K}$. In addition, the electron densities and electron temperatures of such H II regions are computed to vary strongly throughout their volume. To account for this we ran a supplementary set of *Mappings IV* models as described in Dopita et al. (2013) for abundances of 2, 3 and $5Z_{\odot}$ ($12 + \log(\text{O}/\text{H}) = 8.99, 9.17$ and 9.39 respectively) and with a set of fixed pressures in the range $5.0 \leq \log(P/k) \leq 7.0 \text{ Kcm}^{-3}$. This provided a theoretical relationship between $\log(P/k)$ and the actual [S II] $\lambda\lambda 6731/6717$ ratio. This was used to transform the measured [S II] line ratio to a local pressure in each spaxel.

From the line flux data we prepared two abundance-sensitive line ratios described in Dopita et al. (2013);

- [N II] $\lambda 6584$ /[O II] $\lambda\lambda 3727, 9$; and
- [N II] $\lambda 6584$ /[S II] $\lambda\lambda 6717, 31$,

and three excitation-dependent ratios:

- [O III] $\lambda 5007$ /[O II] $\lambda\lambda 3727, 9$,
- [O III] $\lambda 5007$ /[S II] $\lambda\lambda 6717, 31$ and
- [O III] $\lambda 5007$ /H β .

This gives six possible diagnostic plots which are fed through the `pyqz` Python module described in Dopita et al. (2013) to return the computed value of $\log(q)$ and $12 + \log(\text{O}/\text{H})$ for each of the six pairs of line ratios, as well as the mean and standard deviation computed from these. Our `pyqz` Python module (v0.4) is freely available for the community to use under the GNU General Public License (doi:10.4225/13/516366F6F24ED).¹

A complication of this analysis is that the line ratios are a function of pressure in the H II region. The effect of this is mostly to change $[\text{O III}]\lambda 5007/\text{H}\beta$, although other line ratios are affected to lesser degree. As a result, the ionisation parameter derived in high pressure regions may be systematically overestimated. To account for this effect, we ran additional *Mappings IV* models as described by Dopita et al. (2013), for a set of fixed ionisation parameters, $12 + \log(\text{O}/\text{H}) = 8.99, 9.17$ and 9.39 respectively and with a set of (high) pressures in the range $5.0 \leq \log(P/k) \leq 7.0$ Kcm⁻³. The resulting six pairs of line ratios were input to the `pyqz` Python module (v0.4) to solve for both $\log(q)$ and $12 + \log(\text{O}/\text{H})$, and the difference between the values returned and those of the input model were determined. For the abundances, the error was everywhere less than 0.012 dex. However, the error in $\log(q)$, $\Delta \log q$ was much greater. This is displayed in Figure 1. On the basis of these models we have determined an empirical fit to $\Delta \log q$ which provides a satisfactory approximation over the full range of parameters;

$$\Delta \log q = 0.04(\log q - 6.6) [x + 1.5x^{1.8}] \quad (2)$$

where q is the uncorrected value returned by the `pyqz` Python module, and $x = \log(P/k) - 5$. The pressure is determined from the $[\text{S II}]\lambda\lambda 6731/6717$ ratio, as described above. The correction of equation 2 was applied to each spaxel for which the pressure could be measured.

4 Results

4.1 Maps

The maps for some of the objects are given in Figures 2 to 9. These include some points that may be contaminated by shock emission. Such points tend to

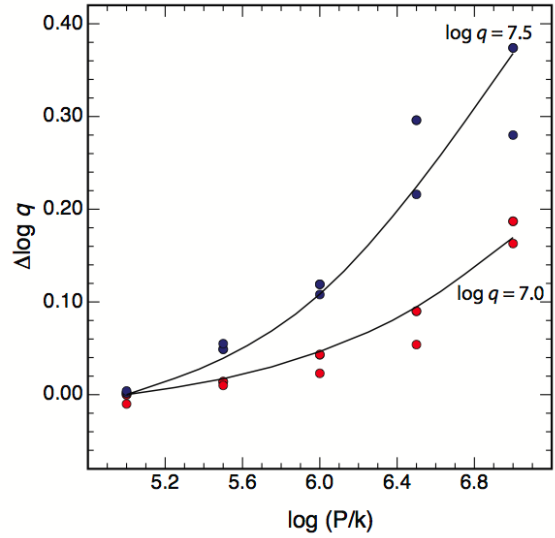


Fig. 1 The overestimate in the logarithmic ionisation parameter $\Delta \log q$ computed as a function of pressure $\log(P/k)$ for three separate abundances (here, the 2 and 3 times solar abundance models overlap). The curves give the empirical fitting formula we have derived, given in equation 2.

show large dispersions in the $12 + \log(\text{O}/\text{H})$ and $\log(q)$ derived from the `pyqz` Python module. For the purpose of plotting the correlations between the derived physical parameters, we exclude all points with a standard deviation of greater than 0.1 dex in $12 + \log(\text{O}/\text{H})$ and/or greater than 0.15 dex in derived $\log(q)$. The resulting correlations are shown for all galaxies in Figures 10 to 12.

4.2 Notes on Individual Objects

F01053-1746 or IC 1623 A/B: This is shown in Figure 2. It is a closely interacting system in the final stages of merging. It is kinematically complex, and shows clear evidence of shock-excited regions as described by Rich, Kewley & Dopita (2011). In this, as in other galaxies, we have removed those spaxels which are obviously shock-excited on the basis of the earlier analysis. The eastern member of the pair (the spaxels on the upper left) is clearly the more metal-rich of the two – a fact which was not evident in the earlier analysis by Rich et al. (2012). However the abundance range is rather restricted, and intrinsic errors in the earlier strong-line techniques used by Rich et al. (2012) (the Pettini & Pagel (2004) method (PP04) scaled to Kewley & Dopita (2002) (KD02) as well as the KD02 diagnostics) would tend to obscure the differences in the oxygen abundance. The separation in metallicity between the two galaxies is clearly evident in the $12 + \log(\text{O}/\text{H})$ vs. $\log(q)$ correlation (see Figure 10). The western galaxy

¹ A digital object identifier (DOI) is a string of character used to uniquely identify an object such as an electronic document. The storage location (a.k.a url) corresponding to a given DOI can be resolved using dedicated websites, such as <http://dx.doi.org> (this tool also allows direct access at <http://dx.doi.org/10.4225/13/516366F6F24ED>)

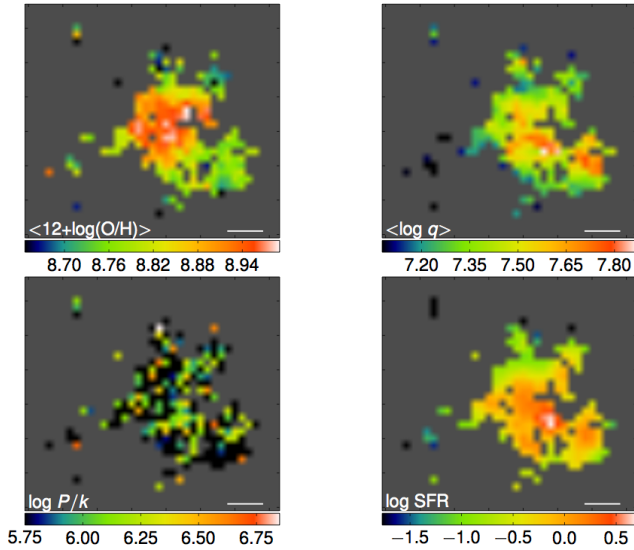


Fig. 2 The spaxel analysis maps of F01053-1746 (IC1623 A/B). Top left: the abundance gradient map, $12+\log(\text{O}/\text{H})$. Top right: the ionisation parameter, $\log(q)$. Bottom left: the local pressure in the ionised plasma, $\log(P/k)$ (pressures below $\log(P/k) \sim 5.7$ cannot be inferred from the $[\text{S II}] \lambda\lambda 6717/6731$ ratio). Bottom right: the star formation rate $\log(\text{SFR})$ in $\text{M}_{\odot}\text{yr}^{-1}\text{kpc}^{-2}$. The short horizontal white bar represents 5 arc sec. on the sky. Note that the correlation between $\log(\text{SFR})$ and $\log(q)$ is better than between $\log(\text{SFR})$ and $12+\log(\text{O}/\text{H})$.

is the more violently star forming of the two, and it also characterised by the highest ionisation parameters. Overall there is a strong correlation between $\log(\text{SFR})$ and $\log(q)$. Little can be learnt from the correlations with H II region pressure.

IRAS 08355-4944: This galaxy (Figure 3) is a post-merger with long remnant tidal tails. Unfortunately there are too few spaxels to make a meaningful map, but the galaxy shows clear correlations between $\log(\text{SFR})$ and both $\log(P/k)$ and $\log(q)$. The ionisation parameter is also correlated with $12 + \log(\text{O}/\text{H})$.

F10257-4339 or NGC 3256: This high-abundance nearby system shown in Figure 4 is another advanced merger displaying widespread evidence of shock-excited gas (Rich, Kewley & Dopita 2011). The measured ionisation parameters show little evidence of variability across the system, being nearly all in the range $7.4 > \log q > 7.0$. For this galaxy (Figure 10) there is a remarkably tight correlation between $\log(\text{SFR})$ and $\log(P/k)$, and also a marked correlation between $12 + \log(\text{O}/\text{H})$ and $\log(P/k)$. The weak abundance gradient found here is in agreement with that found by Rich, Kewley & Dopita (2011).

F13373+0105 E/W or Arp 240: The eastern component of this system shown in Figure 5 is a tidally distorted spiral (see the HST image in Rich, Kewley &

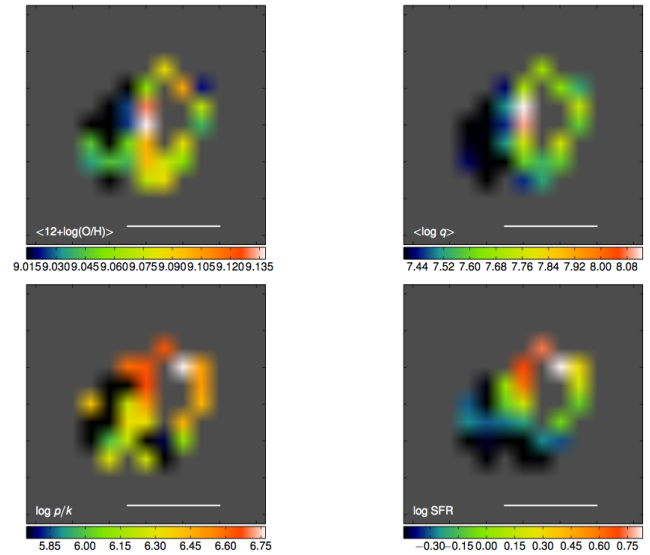


Fig. 3 As figure 1 but for the galaxy IRAS08355-4944.

Dopita (2011)). Mostly the H II gas is too faint to support the spaxel analysis, so the map simply picks out the regions of greatest star formation. These show an approximately constant $\log(q)$ as a function of $\log(\text{SFR})$ (Figure 9). The western component shown in Figure 6 is much more active (Rich et al. 2012), and displays a strong abundance gradient. Our two analyses agree both in the size and the range of this gradient. This object is similar to F01053-1746 in that it displays a strong correlation between $\log(\text{SFR})$ and $\log(q)$ and a bifurcation in the $12 + \log(\text{O}/\text{H})$ vs. $\log(q)$ correlation (Figure 11).

F17222-5953 or ESO 138-G027: This system shown in Figure 7 is a typical, non-interacting, strongly star bursting spiral galaxy. It shows a close correlation between $\log(\text{SFR})$ and $12 + \log(\text{O}/\text{H})$, both of which show a clean radial gradient (Figure 11). There are positive correlations of both these quantities with $\log(q)$, with again a suggestion of bifurcation in these correlations, caused by the enhanced region of star formation seen in the lower left of Figure 7, corresponding to a region north of the nucleus on the sky.

F18093-5744 N/S or IC 4687/4689: These two galaxies are in a close triplet system. IC 4687, shown in Figure 8, is a close merger with the less massive starburst IC 4686. The smaller galaxy IC 4689 (F18093-5744S), Figure 9, interacts with this pair. IC 4687 (Figure 8 and Figure 10) displays a strong and clean positive correlation between both $\log(\text{SFR})$ vs. $\log(q)$ and $12 + \log(\text{O}/\text{H})$ vs. $\log(q)$. IC 4689 (see Figure 8 and Figure 11) shows a correlation in $12 + \log(\text{O}/\text{H})$ vs. $\log(q)$, but any correlation with $\log(\text{SFR})$ (if present) is very weak.

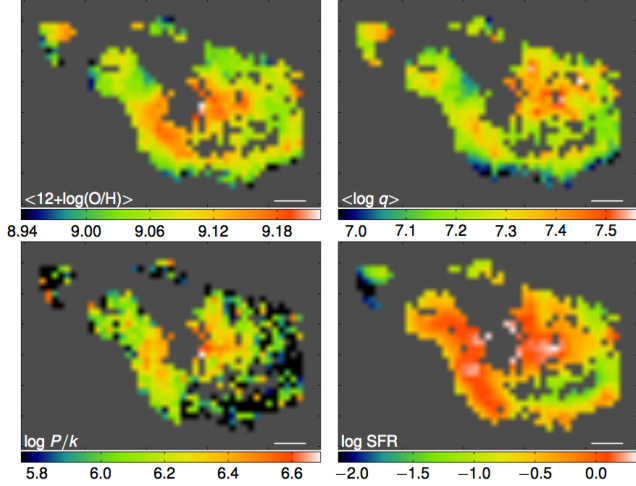


Fig. 4 As figure 1 but for the galaxy F10257-4339 (NGC 3256). Here (unusually) there is a clear correlation between $\log(P/k)$, $\log(\text{SFR})$ and $12 + \log(\text{O}/\text{H})$. However, the observed range of $\log(q)$ is highly restricted.

4.3 Global Correlations

Many of the objects observed show a positive correlation between both $\log(\text{SFR})$ vs. $\log(q)$ and $12 + \log(\text{O}/\text{H})$ vs. $\log(q)$. This is in contrast to observations of H II regions in general; see the data presented in Dopita et al. (2013), for which there is little evidence for any variation in $\log(q)$ with $12 + \log(\text{O}/\text{H})$. Nearly all H II regions fall in a narrow range $7.0 < \log(q) < 7.5$. The outliers tend to be found in lower abundance H II regions, and these have higher, not lower ionisation parameters. It is clear that the starburst galaxies differ in a fundamental manner from normal galaxies, and that these positive correlations of $\log(\text{SFR})$ vs. $\log(q)$ and $12 + \log(\text{O}/\text{H})$ vs. $\log(q)$ demand some theoretical explanation.

Several of the objects shown in Figure 10) and 11 show both positive correlations not only between $\log(q)$ and $\log(\text{SFR})$ but also between $\log(q)$ and $12 + \log(\text{O}/\text{H})$. Do these then drive a correlation between $12 + \log(\text{O}/\text{H})$ and $\log(\text{SFR})$? We test this in Figure 14

5 Interpretation of Results

The possible explanations for a systemic increase in the ionisation parameter in regions of high star formation density are as follows:

1. The shape of the stellar Initial Mass Function (IMF) is changing with $\log(\text{SFR})$. The harder radiation field produced by a flatter IMF could then masquerade as if it were a higher ionisation parameter.

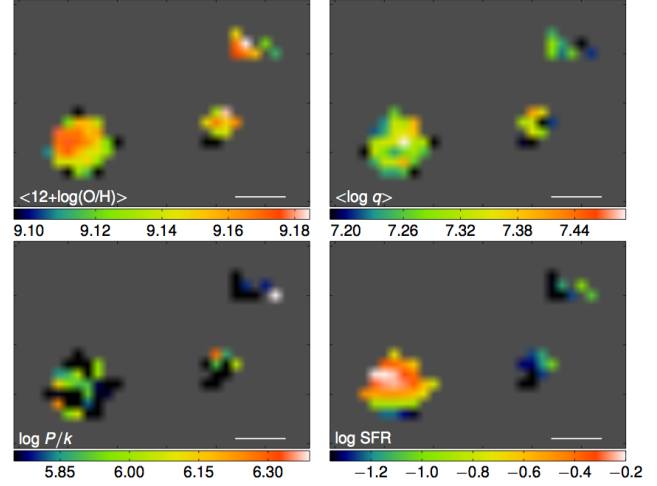


Fig. 5 As figure 1 but for the object F13373+0105E, a component of Arp240.

2. The mean cluster mass M_{cl} systematically increases with $\log(\text{SFR})$. The collective effects of a massive cluster speed up the expansion of the surrounding H II region, and produce a higher ionisation parameter at a given cluster age.
3. The H II regions may overlap each other.
4. The structure of the H II regions is dependent on the physical environment of the starburst region.

We will now explore each of these possibilities in turn.

5.1 Effect of IMF slope

In order to check the effect of an environment dependent IMF slope, we have run a new set of Starburst 99 v6.0.2 (Leitherer et al. 1999) models with continuous star formation extending over 3Myr - typical of the distribution of ages in massive young clusters exciting the most luminous H II regions (Beccari et al. 2010; De Marchi et al. 2011). These models have different slopes of the upper ($0.5 - 120 M_{\odot}$) IMF; -2.6, -2.2, -1.8 and -1.4. To be as closely comparable to the models used by Dopita et al. (2013) as possible, we used the Geneva tracks for metallicity $Z=0.04$, and the Lejeune, Cuisinier, & Buser (1997) model atmospheres. For stars with strong winds we switch to the Schmutz, Leitherer, & Gruenwald (1992) extended model atmospheres using the prescription of Leitherer & Heckman (1995).

These atmospheres were input into the Mappings IV code (Dopita et al. 2013). We ran isobaric models with a pressure of $\log(P/k) = 10^6 \text{cm}^{-3} \text{K}$, typical of our starbursts, a 3 times solar abundance set (oxygen abundance $12 + \log(\text{O}/\text{H}) = 9.17$) and input ionisation parameters of $q = 6.9, 7.15, 7.4$ and 7.65 . The resultant spectra were then fed through the pyqz software

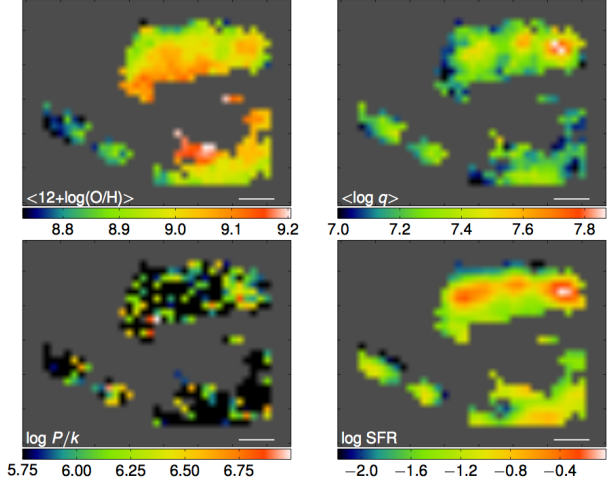


Fig. 6 As figure 1 but for the object F13373+0105W, a component of Arp240. This is a large barred spiral galaxy, with very little gas near the nucleus (roughly in the centre of the image). Again, the correlation between $\log(\text{SFR})$ and $\log(q)$ is better than between $\log(\text{SFR})$ and $12 + \log(\text{O}/\text{H})$.

(Dopita et al. 2013) to solve for the apparent (output) ionisation parameter and the chemical abundance. This procedure recovered the input abundances within 0.05 dex, but the output $\log q$ was somewhat different from the input value. The result is shown in Figure 15.

The effect of the IMF slope is rather small. Of course we have controlled against first order effects by choosing the ionisation parameter at the inner edge of the nebula. Any residual effect is due to changes in the shape of the ionising radiation field. The somewhat harder radiation field of the flatter IMF does indeed raise the derived $\log q$, but only by about 0.1 dex at most. However, this effect tends to reverse at the highest input values of $\log q$ due to the different temperature structure of the nebula, which shows steep temperature gradients through the models at the high chemical abundances characterising our model H II regions. We conclude that IMF variations which are a function of the local star formation rate cannot explain the size of our derived correlation between $\log q$ and $\log(\text{SFR})$.

5.2 Spherical H II regions: Effect of cluster mass

Dopita et al. (2006) developed a simple theory describing the development of a spherical H II region trapped between the outer boundary of an expanding bubble powered by the wind from the central cluster, and the shocked stellar wind itself. In this idealised model, the pressure in the H II region is supplied by the pressure of the shocked stellar wind. The central cluster provides the EUV photons which ionise the nebula, while the temporal evolution of the bubble (determined by

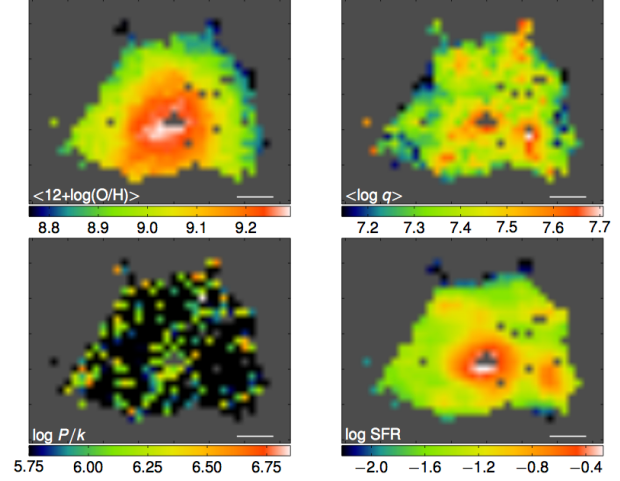


Fig. 7 As figure 1 but for the object F17222-5953 (ESO 138-G027).

the mechanical energy luminosity of the central cluster, and the density of the interstellar medium) fixes the radius. In this theory, the ionisation parameter at the contact discontinuity in the photoionised plasma depends simply on the instantaneous properties of the exciting cluster stars;

$$q(t) \propto \delta(t)^{3/2} S_*(t) / L_{\text{mech}}(t), \quad (3)$$

where $\delta(t)$ is the instantaneous ratio of the density in the H II region to the density in the interstellar medium (ISM) surrounding the H II region, $S_*(t)$ is the instantaneous flux of ionising photons produced by the central cluster, and $L_{\text{mech}}(t)$ is the instantaneous mechanical energy flux from the cluster. Clearly, the ratio of two main terms in Equation 3, $S_*(t) / L_{\text{mech}}(t)$, is unique for a given slope of the upper IMF, α_3 , and for a given stellar metallicity. Provided that these variables are fixed, the $\delta(t)$ term provides for a weak coupling between $q(t)$, the mean cluster mass, M_{cl} , and the pressure in the interstellar medium, P_0 ; $q \propto (M_{\text{cl}} / P_0)^{1/5}$. This scaling is evident in Figure 5 of Dopita et al. (2006).

Dopita et al. (2006) also showed that the ionisation parameter is rather sensitive to the chemical abundance, Z . At high abundance the stellar wind has higher opacity, and absorbs ionising photons before they escape the extended atmosphere, and the mechanical luminosity is higher leading to greater compression of the H II shell. Both of these effects lower q leading to $q \propto Z^{-0.8}$, approximately over the whole range of abundance, although the abundance effect is much weaker at the high chemical abundances characterised by these objects. Note however that we have found a *positive* correlation between q and $12 + \log(\text{O}/\text{H})$ - exactly the opposite of what is predicted by theory.

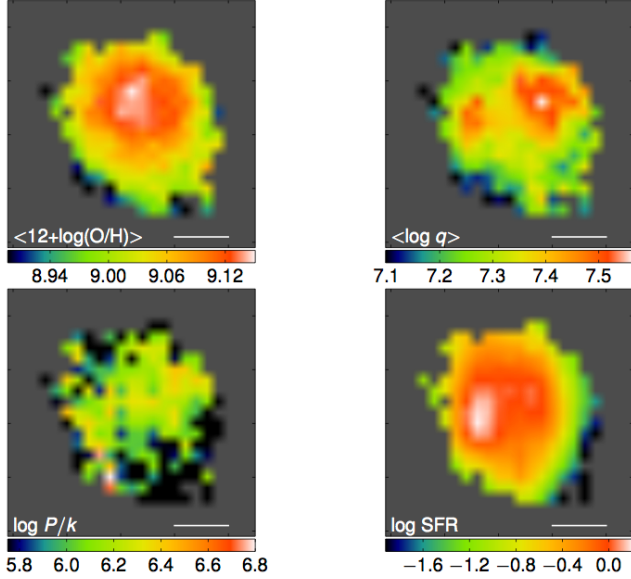


Fig. 8 As figure 1 but for the object F18093-5744N (IC 4687). This shows clean correlations between $\log(\text{SFR})$, $\log(q)$ and $12+\log(\text{O}/\text{H})$.

The pressure effect on q predicted in the theory can be readily removed, since we have already measured the pressure in most spaxels. We take $\log(p/k) = 5$ as the reference pressure, since all of our photoionisation models use this as the default, and we correct the measured q by the amount given by the theory; a factor $[(P/k)/10^5 \text{cm}^{-3} \text{K}]^{1/5}$. Since, in general, the measured pressure in any spaxel is higher than $\log(p/k) = 5$, the effect of correcting for pressure in this way serves to increase the effective q . This tends to reverse the correction accounting for the change in the line ratios with pressure (see Section 3). The result is shown in Figure 13 for the six objects for which many spaxels have been measured. For each of these, we also show in pale the distribution of all measured points. In general, we now have a *positive* correlation between q and star formation for all galaxies, although there seems to be a threshold in star formation rate (which differs galaxy to galaxy) above which the correlation becomes strong. Where the strong correlation exists:

$$q \propto \text{SFR}^{0.34 \pm 0.08}. \quad (4)$$

There is some evidence of a threshold value for $\log q \sim 7.2 - 7.4$ below which this correlation disappears. Coincidentally (or not?) this is the value of $\log q$ which characterises most individual extragalactic H II regions (Dopita et al. 2013).

If we adopt the mass-loss bubble driven model of the evolution of H II regions from Dopita et al. (2006), then the relation between cluster mass and ionisation

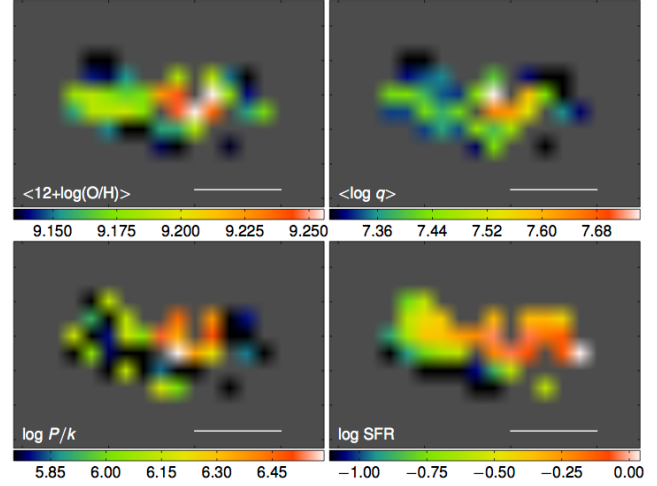


Fig. 9 As figure 1 but for the object F18093-5744S (IC4689). Despite the relatively small number of spaxels in this object, all quantities plotted seem to be correlated.

parameter is $q \propto M_{cl}^{1/5}$. This is a very weak dependence and implies that large variations of cluster mass as a function of star formation density are needed to drive the observed variation in $\log q$. We derived above that $q \propto \Sigma_{\text{SFR}}^{0.34 \pm 0.08}$, where the star formation rate is now written as Σ_{SFR} to emphasise that we are talking about surface rates of star formation. If the simple spherical evolution model is applicable, and if the star formation rate *vs.* q correlation is entirely driven by a change in mean cluster mass, these relations together imply that $M_{cl} \propto \Sigma_{\text{SFR}}^{1.7 \pm 0.4}$.

If, for example, the mean cluster mass at a star formation rate of $0.1 \text{ M}_{\odot} \text{yr}^{-1} \text{kpc}^{-2}$ is 10^4 M_{\odot} , then for a region with $3.0 \text{ M}_{\odot} \text{yr}^{-1} \text{kpc}^{-2}$, the mean cluster mass would rise to $3 \times 10^6 \text{ M}_{\odot}$. Such values are not forbidden according to the arguments of the previous sub-section. Indeed, in the case of one of our objects, F10257-4339 or NGC 3256, a survey of its clusters by Trancho et al. (2007) finds that they have masses in the range $0.2 - 4 \times 10^6 \text{ M}_{\odot}$. In other galaxies even more massive clusters are found. For example, in NGC 7252 and NGC 1316 clusters have been found with masses significantly above 10^7 M_{\odot} (Schweizer & Seitzer 1998; Maraston et al. 2004; Bastian et al. 2006).

The idea that cluster masses scale up with star formation rates has some support from a number of observational and theoretical papers. Most directly, the mass function of clusters has been found by a number of authors to follow a Schechter (1976) distribution,

$$dN/dM = AM^{-\beta} \exp[-M/M_*], \quad (5)$$

where $\beta \sim 2$, and M_* is the cut-off mass. For ordinary disk galaxies, $M_* \approx 2 \times 10^5 \text{ M}_{\odot}$ (Gieles et al. 2006;

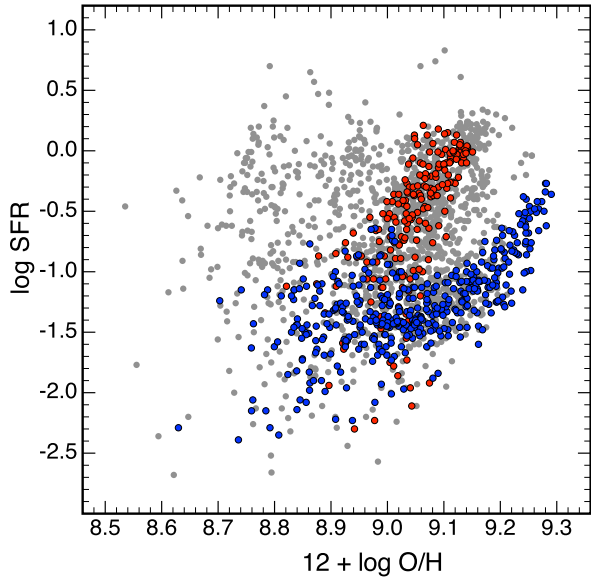


Fig. 14 The global correlation between $12 + \log(\text{O}/\text{H})$ and $\log(\text{SFR})$. For the sample as a whole, we find little evidence that these are correlated, but for individual objects such as F17222-5953 (blue points) or F18093-5744 N (red points) there is a strong correlation. These galaxies display strong abundance gradients, as well as increasing star formation rates towards their centres, presumably associated with higher surface densities of gas.

Larsen 2009), while for luminous IR galaxies, Bastian et al. (2008) finds $M_* \approx 10^6 M_\odot$; (Portegies et al. 2010). However, other studies such as that by Chandar et al. (2010) find no evidence for an upper mass cutoff.

This idea was recently developed on a theoretical basis by Powell et al. (2013). They studied merger-induced star formation with 5 pc resolution adaptive mesh refinement simulations of low-redshift equal-mass mergers with randomly chosen orbital parameters. They found an enhanced mass fraction of very dense gas that appears as the gas density probability density function evolves during the merger, which opens up the possibility that such dense regions may give rise to more massive clusters. Powell et al. (2013) argue that this dense gas may reveal itself in terms of the enhanced HCN(1-0)/CO(1-0) ratios which are observed in ULIRGs (Juneau et al. 2009). Simulations at even higher resolution by Hopkins et al. (2013) lead to similar conclusions. They find that the final starburst is dominated by in situ star formation, fuelled by gas which flows inwards due to global torques. High gas density results in massive giant molecular clouds, and rapid star formation leading to the formation of super star clusters with masses of up to $10^8 M_\odot$.

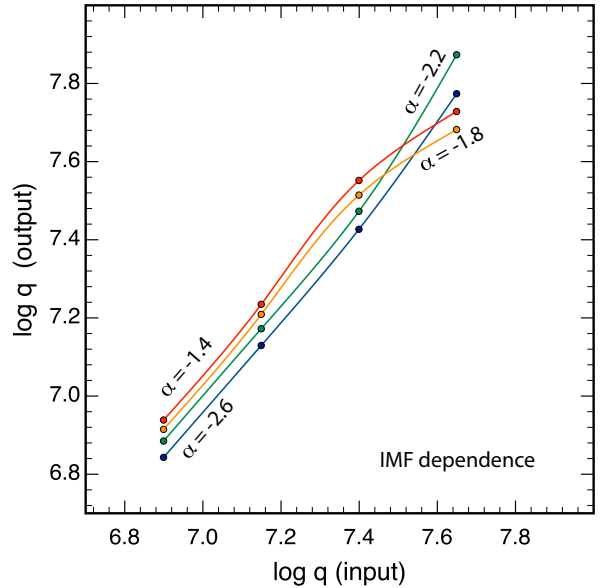


Fig. 15 The $\log q$ input into the *Mappings IV* code vs. the output $\log q$ as determined by the *pyqz* software (Dopita et al. 2013). Four different input IMF were used with upper IMF slopes of $\alpha = -2.6, -2.2, -1.8$ and -1.4 , respectively. The IMF slope has only a small effect on q , and IMF variations alone cannot explain the correlation between $\log(\text{SFR})$ and $\log(q)$.

Our simple spherical model of H II region evolution implies that the surface number density of clusters has to decrease as the surface density of gas increases. Crudely speaking, $\Sigma_{\text{SFR}} \propto \Sigma_{cl} M_{cl}$, where Σ_{cl} is the surface number density of young clusters. Given that the Kennicutt (1998) star formation law has $\Sigma_{\text{SFR}} \propto \Sigma_g^{1.4 \pm 0.1}$, where Σ_g is the gas surface density, and that $M_{cl} \propto \Sigma_{\text{SFR}}^{1.7 \pm 0.4}$, then we have that $\Sigma_{cl} \propto \Sigma_g^{-1}$, approximately. Thus dense regions should have fewer clusters, but individually they would be much more massive. As pointed out by our referee, this is in direct contradiction to observation, since the density of clusters does not decrease in this manner. Galaxies with the highest gas densities (e.g., NGC 3256, Arp 220, and to a lesser extent the Antennae galaxies) also have more clusters, and the clusters are strongly positively correlated with the gas with individual galaxies Zhang, Fall & Whitmore (2001). So higher gas surface densities lead to more clusters. This result also comes out of the analytic calculations of Kruijssen et al. (2012), although in his model, the clusters are also destroyed faster due to the high gas densities (within a few Myrs) so there is a “sweet spot” for surviving clusters.

In conclusion, while cluster masses may indeed vary as a function of star formation density, this effect is not by itself sufficient to drive the observed slope of the

$\log q$: $\log(\text{SFR})$ relation. We must therefore appeal to geometrical effects. These include of either the effect of overlapping H II regions, or more realistic non-spherical geometries of the H II regions.

5.3 H II region overlap

One possible way of changing the effective $\log q$ in the H II regions is to make them interfere spatially with each other, which would put ionised gas closer to the ionising source. However, it is not necessarily the case that this would enhance the $\log q$ in the ionised gas, since the external pressure of the ionised gas is determined by the pressure of the OB-star stellar wind of the exciting cluster. A reduction in the effective radius of the H II region will lead not only to an increase in the photon flux, but also to a corresponding increase in the confining pressure, which would tend to keep $\log q$ fixed. The degree to which this statement is true will depend on the position of the inner shock, where the kinetic energy of the stellar wind is thermalised, and whether the ionised material lies within or without the inner shock. Putting these issues of detail aside, let us first consider whether in principle the H II regions in violently star-bursting regions can become so closely packed that they can run into each other.

The peak star formation in our objects approaches $3.0 \text{ M}_{\odot}\text{yr}^{-1}\text{kpc}^{-2}$. If all of this were to occur in a single cluster over the $\sim 3 \text{ Myr}$ that the cluster produces a strong UV radiation field, then the maximum cluster mass could reach $M_{cl} \approx 10^7 \text{ M}_{\odot}$. Of course, the star formation is much more likely to be distributed amongst a number of smaller clusters. Typical H II region parameters have $\log(P/k) \sim 6.2 \text{ cm}^{-3}\text{K}$ and $\log q \sim 7.5 \text{ cm s}^{-1}$. With these parameters, the H II region forms a thin ionised shell around the hot shocked stellar wind, and the radius of the H II region is determined by the value of $\log q$. The radius scales as the square root of the cluster luminosity or cluster mass. From detailed *Mappings IV* photoionisation models:

$$R_{\text{HII}} = 68[M_{cl}/10^6 \text{ M}_{\odot}]^{1/2} \text{ pc.} \quad (6)$$

Thus, the maximum volume of the stellar wind plus H II region is achieved when all of the star formation is concentrated in a single cluster. This volume is $\sim 4 \times 10^7 \text{ pc}^3$. However the total volume available is $10^8 - 10^9 \text{ pc}^3$, depending on whether the available thickness of the gas layer is 100pc or 1.0kpc. We conclude that, at the high pressures characteristic of these starburst regions, interference between the individual H II regions around clusters is rather unlikely to occur.

5.4 Non-spherical H II regions.

The approximation of spherical H II region expansion is clearly too simplistic. The interstellar medium of galaxies is turbulent and fractal, and regions of active star formation are constantly shifting to where dense molecular clouds are actively collapsing. Where dense molecular clouds are overrun by the expanding shell of ionised gas, “elephant trunks” are formed, each surrounded by an outflowing photo-evaporation zone. In some cases, an embedded H II region breaks out into a lower density region, forming a “champagne flow” (Tenorio-Tagle 1979; Arthur 2007; Hu & Lu 2008).

In the case of a champagne flow, very high ionisation parameters can occur since the molecular gas remains very close to the ionising source, limited only by the photo-ablation timescale of the molecular cloud. Something of this kind may be occurring in M82. Smith et al. (2006) and Westmoquette et al. (2007) used HST imaging and spectroscopic analysis of super star clusters in M82 and found that the most compact region A1 contains a massive ($\sim 0.5 - 1 \times 10^6 \text{ M}_{\odot}$) young (6 – 7Myr) and compact ($\sim 3.5 \text{ pc}$ radius) cluster, but hosts a HII region around it with a size of only 4.5 pc. This H II region has an internal pressure of $P/k = (1 - 2) \times 10^7 \text{ cm}^{-3}\text{K}$ and with an ionisation parameter $\log q \sim 8.2 \text{ cm s}^{-1}$ ($\log U \sim -2.2$). The high ionisation parameter is observed to extend over a region 500 pc across. Thus, the whole region seems to represent a (more extreme) version of the high - q , high - SFR regions studied in this paper.

We should first note that the measured value of the ionisation parameter for this object corresponds to the limit set by where the radiation pressure (acting mainly on dust) exceeds the gas pressure at the inner edge of the ionised region closest to the exciting stars. In this case radiation pressure serves to compress the ionised gas close to the ionisation front (Dopita et al. 2002) and dust becomes the main absorber of the ionising photons (Dopita et al. 2003).

The ionised region around the cluster A1 cannot be spherical. Compared with the example given by equation 6, the higher pressure alone leads to a 25 times reduction in the Strömgren volume, and the absorption of the ionising photons by dust ($\sim 70\%$), makes the total reduction in the Strömgren volume a factor of 80. Nonetheless, we would still expect the H II region to have a radius $\sim 10 - 15 \text{ pc}$ in radius, compared to the 4.5pc observed. Thus, either it is a “blister” H II region at the edge of a massive molecular cloud, or else it contains massive molecular clouds much closer to the central stars than the spherical shell model would predict. Either way, the nebular geometry is distinctly non-spherical.

Smith et al. (2006) and Westmoquette et al. (2007) suggest that the expansion of the H II region is “stalled” by the dense environment. However, the concept of stalling the expansion is dubious, since the internal pressure of the H II region from ionised plasma, stellar winds and supernova explosions will always exceed the pressure in the ISM, for any reasonable values. The fundamental question is whether the expansion velocity is supersonic or subsonic with respect to the turbulent velocity of the neutral (or molecular) medium. The possibility that the expansion velocity of the H II region during the lifetime of the OB stars within it may be less than the characteristic random velocity of the molecular clouds in its vicinity opens up the interesting possibility that the molecular clouds may “fall” into the H II region and become highly ionised (high- q) as they pass close to the exciting stars. In this geometry, not only do we have a Kelvin-Helmholtz unstable layer at the surface of the clouds which leads to a turbulent outflow, but in the high- q conditions produced, we may also have radiative acceleration acting on dust, which can lead to high outflow velocities (Dopita et al. 2002). Indeed Westmoquette et al. (2007) conclude that (quoting their paper):

Evaporation and /or ablation of material from interstellar gas clouds caused by the impact of high-energy photons and fast flowing cluster winds produce a highly turbulent layer on the surface of the clouds from which the emission arises.

Molecular clouds may also be infalling towards the stars as part of a general accretion flow, provided that the mass of the central cluster and its placental molecular cloud complex is large enough.

In order to check whether the clouds can cross the H II region within the lifetime of the OB stars, we have used the mass-loss bubble driven model of the evolution of H II regions from Dopita et al. (2006) to compute the expansion timescale of the bubble, and the infall timescale of a cloud from the edge of the bubble to the centre, assuming a turbulent cloud velocity of 15 km s⁻¹, similar to the velocity dispersions inferred by direct observation (Dickey et al. 1990) or theory (Joung et al 2009). The results are plotted in Figure 16 for two cluster masses and H II region pressures. For an appreciable fraction of the lifetime, the infall timescale is less than the expansion timescale. Lower cluster masses, and higher pressures both favour the infall of molecular clouds. Thus, in dense starburst regions, the dynamical evolution of the molecular gas around the H II region cannot be ignored.

6 Conclusions

We conclude that the spaxel analysis of data cubes obtained in luminous infrared galaxies provides useful measures of the local chemical abundance, ionisation parameter, gas pressure and star formation rates. Positive correlations are found between the ionisation parameter and either the star formation rate or the local

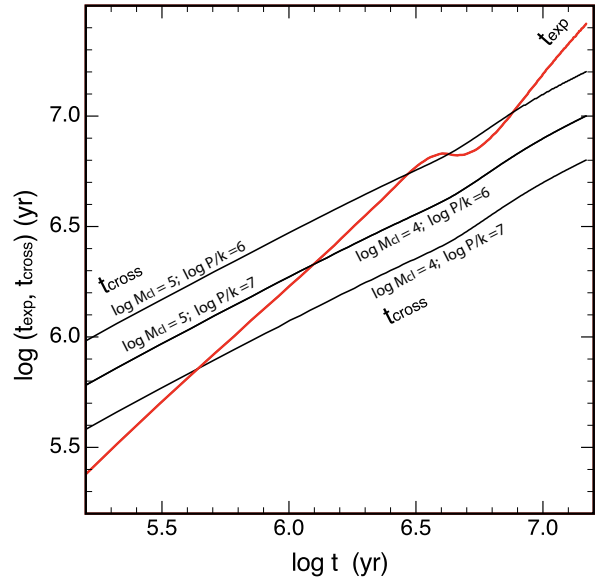


Fig. 16 The expansion timescale of a (spherical) H II region compared with the infall timescale of molecular clouds in a turbulent ISM. The infall timescale maybe appreciably smaller than the expansion timescale once the H II region is older than about 10⁶yr.

chemical abundances. We expect star formation rates and chemical abundances to be correlated, since the inner regions of these galaxies generally have both higher star formation rates and higher chemical abundances than the outskirts. However, the fact of a correlation of these quantities with ionisation parameter is more intriguing. We have corrected for the effect of the local pressure, but this only serves to make the q : SFR correlation stronger, as shown in Figure 12.

We have examined a number of possible causes for the correlation;

- That initial mass function variation drives the correlations.
- That the mass of the exciting cluster changes systematically with environment.
- That in high star formation regions, overlap of the H II regions occurs.
- That the geometry of the molecular and ionised gas changes strongly with environment.

We are able to eliminate the first and third of the possibilities listed above. While the mass of the exciting clusters may well become higher as the star formation rate per unit area becomes higher, this effect is insufficient to drive the observed correlation. We conclude that the geometrical effect is the most likely cause, and that the H II regions in the dense star forming regions

contain inclusions of molecular clouds undergoing violent radiation pressure dominated photo-ablation close to the exciting stars, analogous to that described by Smith et al. (2006); Westmoquette et al. (2007) in the nuclear region of M82. In these circumstances, fast radially-directed outflows from the molecular clouds can be driven by radiative pressure. This property may well be the root cause of the correlation between the turbulent width of the H α line and the H α luminosity found by many authors e.g. Green et al. (2010); Wisnioski et al. (2012) and Swinbank et al (2012).

The model of radiation pressure dominated photo-ablation of dense molecular clouds embedded deep within H II regions in high specific star formation regions should give rise to consequences amenable to direct observation. First, the clouds themselves should be visible in high-resolution H α images taken with the Hubble Space Telescope. A good example of such an environment is M83, where the central pressure and star formation rate achieve values comparable with the cores of the ULIRGs studied here; *c.f.* Dopita et al. (2010b). In addition, in these objects high-resolution integral field spectroscopy (either in the IR or at optical wavelengths) should reveal local line broadening due to the high-velocity comet-like ablation flows expected at the edges of the dense molecular inclusions. A more extreme example of such a flow has been observed with HST in the nearby Seyfert 2 galaxy, NGC 1068 (Cecil et al. 2002). Here the outflow velocities range up to thousands of km s⁻¹, while for the photoablation flows we are considering velocities would be much lower; ~ 100 km s⁻¹.

Acknowledgements Mike Dopita and Lisa Kewley acknowledge the support of the Australian Research Council (ARC) through their Discovery project DP130103925 This work was also funded by the Deanship of Scientific Research (DSR), King Abdulaziz University, under grant No. (5-130/1433 HiCi). The authors acknowledge this financial support from KAU. We also thank the anonymous referee for insightful comments which led us to re-examine our fundamental assumptions. The paper has been much improved as a result of this valuable input.

References

- Adamo, A., Östlin, G., Zackrisson, E., Hayes, M., Cumming, R. J., Micheva, G. 2010, Mon. Not. R. Astron. Soc., 407, 870
- Andrews, J. E. et al., 2013, *Astrophys. J.*, 767, 51
- Armus, L. et al. 2009, *Publ. Astron. Soc. Pac.*, 121, 559
- Arthur, S. J. 2007, *Astrophys. J.*, 670, 471
- Bastian, N., Saglia, R. P., Goudfrooij, P., Kissler-Patig, M., Maraston, C., Schweizer, F., & Zoccali, M., 2006, *Astron. Astrophys.*, 448, 881
- Bastian, N., Gieles, M., Goodwin, S. P., Trancho, G., et al. 2008, *Mon. Not. R. Astron. Soc.*, 389, 223
- Beccari, G et al. 2010, *Astrophys. J.*, 720, 1108
- Bekki, K. & Meurer, G. R., 2013, *Astrophys. J. Lett.*, 765, 22
- Cappellari, M. et al. 2012, *Nature*, 484, 485
- Cecil, G. , Dopita, M. A., Groves, B. , Wilson, A. S., Ferruit, P., Pécontal, E., & Binette, L. 2002, *Astrophys. J.*, 568, 627
- Chandar, R. et al. 2010, *Astrophys. J.*, 719, 966
- De Marchi, G. et al. 2011, *Astrophys. J.*, 739, 27
- Dickey, J. M., Hanson, M. M., & Helou, G. 1990, *Astrophys. J.*, 352, 522
- Dopita, M.A. & Ryder, S.D. 1994, *Astrophys. J.*, 430, 163.
- Dopita, M. A., Fischera, J., Sutherland, R. S., Kewley, L. J., Tuffs, R. J., Popescu, C. C., van Breugel, W., Groves, B. A., & Leitherer, C. 2006, *Astrophys. J.*, 647, 244
- Dopita, M. A., Groves, B. A., Sutherland, R. S., Binette, L. & Cecil, G. 2002, *Astrophys. J.*, 572, 753
- Dopita, M. A., Groves, B. A., Sutherland, R. S., & Kewley, L. J. 2003, *Astrophys. J.*, 583, 727
- Dopita, M., Hart, J., McGregor, P., Oates, P., Bloxham, G., & Jones, D. 2007, *Ap&SS*, 310, 255
- Dopita, M., Rhee, J., Farage, C., McGregor, P., Bloxham, G., Green, A., Roberts, B., Neilson, J., Wilson, G., Young, P., Firth, P., Busarello, . & Merluzzi, P. 2010, *Ap&SS*, 327, 245
- Dopita, M. A. et al. 2010, *Astrophys. J.*, 710, 964
- Dopita, M. A., Sutherland, R. S., Nicholls, D. C., Kewley, L. J., & Vogt, F. P. A. 2013, *Astrophys. J. Suppl. Ser.*, accepted.
- Gieles, M, Larsen, S. S., Scheepmaker, R. A., Bastian, N., Hass, M. R., & Lamers, H. J. G. L. M., 2006, *Astron. Astrophys.*, 446, L9.
- Green, A. W., Glazebrook, K., McGregor, P.J., Abraham, R. G., Poole, G. B., Damjanov, I., McCarthy, P. J., Colless, M. & Robert G. Sharp, R.G. 2010, *Nature*, 467, 684
- Hopkins, P. F., Cox, T. J.; Hernquist, L., Narayanan, D., Hayward, C. C., & Murray, N., 2013, *Mon. Not. R. Astron. Soc.*, 430, 1901
- Hoversten, E. A., & Glazebrook, K. 2008, *Astrophys. J.*, 675, 163
- Joung, M. R., Mac Low, M-M., & Bryan, G. L. 2009, *Astrophys. J.*, 704, 137
- Juneau, S., Narayanan, D. T., Moustakas, J., Shirley, Y. L., Bussmann R. S., Kennicutt, Jr. R. C., & Vanden Bout, P. A., 2009, *Astrophys. J.*, 707, 1217
- Hu, Ren-Yu & Lou, Yu-Qing 2008, *Mon. Not. R. Astron. Soc.*, 390, 1619
- Kennicutt, R.C. Jr. 1998, *Annu. Rev. Astron. Astrophys.*, 36, 189.
- Kewley, L. J. & Dopita, M. A. 2002, *Astrophys. J. Suppl. Ser.*, 142, 35
- Kruijssen, J. M. D., Pelupessy, F. I., Lamers, Henny J. G. L. M., Portegies Zwart, S. F., Bastian, N., & Icke, V. 2012, *Mon. Not. R. Astron. Soc.*, 421, 1927
- Larsen, S. S., 2009, *Astron. Astrophys.*, 494, 539.
- Le Floc'h, E et al. 2005, *Astrophys. J.*, 632, 169

- Leitherer, C., & Heckman, T. M. 1995, *Astrophys. J. Suppl. Ser.*, 96, 9
- Leitherer, C., Schaerer, D., Goldader, J. D., Delgado, R. M. G., Robert, C., Kune, D. F., de Mello, D. F., Devost, D & Heckman, T. M., et al. 1999, *Astrophys. J. Suppl. Ser.*, 123, 3
- Lejeune, Th., Cuisinier, F., & Buser, R. 1997, *Astron. Astrophys. Suppl. Ser.*, 125, 229
- Magnelli, B., Elbaz, D., Chary, R. R., Dickinson, M., Le Borgne, D., Frayer, D. T., & Willmer, C. N. A. 2011, *Astron. Astrophys.*, 528, A35
- Maraston, C., Bastian, N., Saglia, R. P., Kissler-Patig, M., Schweizer, F., & Goudfrooij, P. 2004, *Astron. Astrophys.*, 416, 467
- Meurer, G. R., et al. 2009, *Astrophys. J.*, 695, 765
- Pettini, M. & Pagel, B. E. J. 2004, *MNRAS*, 348, L59
- Powell, L. C., Bournaud, F., Chapon, D., Teyssier, R. 2013, *Mon. Not. R. Astron. Soc.*, 434, 1028
- Portegies Z., Simon F., McMillan, S. L. W.; Gieles, M. 2010, *Annu. Rev. Astron. Astrophys.*, 48, 43
- Rich, J. A., Dopita, M. A., Kewley, L. J. & Rupke, D. S. N., 2010, *Astrophys. J.*, 721, 505
- Rich, J. A., Kewley, L. J., & Dopita, M. A., 2011, *Astrophys. J.*, 734, 87
- Rich, J. A., Torrey, P., Kewley, L. J., Dopita, M. A., Rupke, D. S. N., 2012, *Astrophys. J.*, 753, 5
- Sanders, D. B., Mazzarella, J. M., Kim, D., Surace, J. A., & Soifer, B. T. 2003, *Astron. J.*, 126, 1607
- Schechter, P., 1976, *Astrophys. J.*, 203, 297
- Schmutz, W., Leitherer, C., & Gruenwald, R. B. 1992, *Publ. Astron. Soc. Pac.*, 104, 1164
- Schweizer, F., & Seitzer, P. 1998, *Astron. J.*, 116, 2206
- Smith, L. J., Westmoquette, M. S., Gallagher, J. S., O'Connell, R. W., Rosario, D. J., & de Grijs, R. 2006, *Mon. Not. R. Astron. Soc.*, 370, 513
- Swinbank, A. M., Smail, I., Sobral, D., Theuns, T., Best, P. N., & Greach, J. E. 2012, *Astrophys. J.*, 760, 130
- Tenorio-Tagle, G. 1979, *Astron. Astrophys.*, 71, 59
- Trancho, G., Bastian, N., Miller, B. W., & Schweizer, F. 2007, *Astrophys. J.*, 664, 284
- Treu, T., Auger, M. W., Koopmans, L. V. E., Gavazzi, R., Marshall, P. J., & Bolton, A. S. 2010, *Astrophys. J.*, 709, 1195
- van Dokkum, P. G. 2008, *Astrophys. J.*, 674, 29
- Weidner, C., Kroupa, P., & Pflamm-Altenburg, J. 2011, *Mon. Not. R. Astron. Soc.*, 412, 979
- Westmoquette, M. S., Smith, L. J., Gallagher, J. S. III., O'Connell, R. W., Rosario, D. J., & de Grijs, R. *Astrophys. J.*, 671, 358
- Wisnioski, E., Glazebrook, K., Blake, C., Poole, G. B., Green, A. W., Wyder, T. & Martin, C. 2012, *Mon. Not. R. Astron. Soc.*, 422, 3339
- Zhang, Qing, Fall, S. M., & Whitmore, B. C., 2001, *Astrophys. J.*, 561, 727

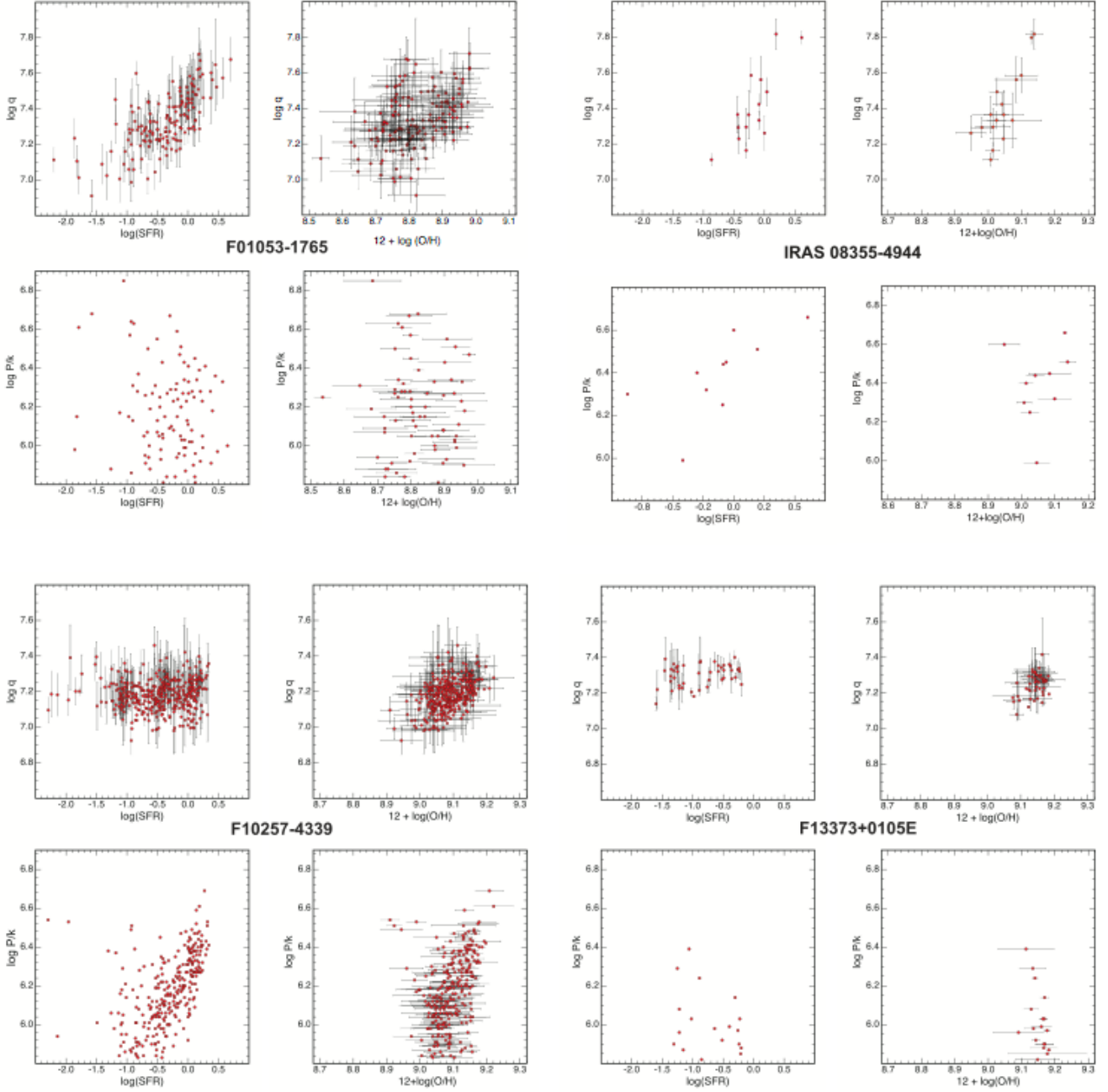


Fig. 10 Correlations for F01053-1746 (IC1623 A/B), IRAS08355-4944, F10257-4339 (NGC 3256) and F13373+0105E. For each of these the panels are, top left: the $\log(\text{SFR})$ vs. $\log(q)$ correlation. Here and elsewhere, $\log(\text{SFR})$ should be read as the surface rate of star formation $\log(\Sigma_{\text{SFR}})$, measured in units of $M_{\odot}\text{yr}^{-1}\text{kpc}^{-2}$. Top right: the $12+\log(\text{O}/\text{H})$ vs. $\log(q)$ correlation. Bottom left: $\log(\text{SFR})$ vs. $\log(P/k)$ correlation. Bottom right: the $12+\log(\text{O}/\text{H})$ vs. $\log(P/k)$ correlation.

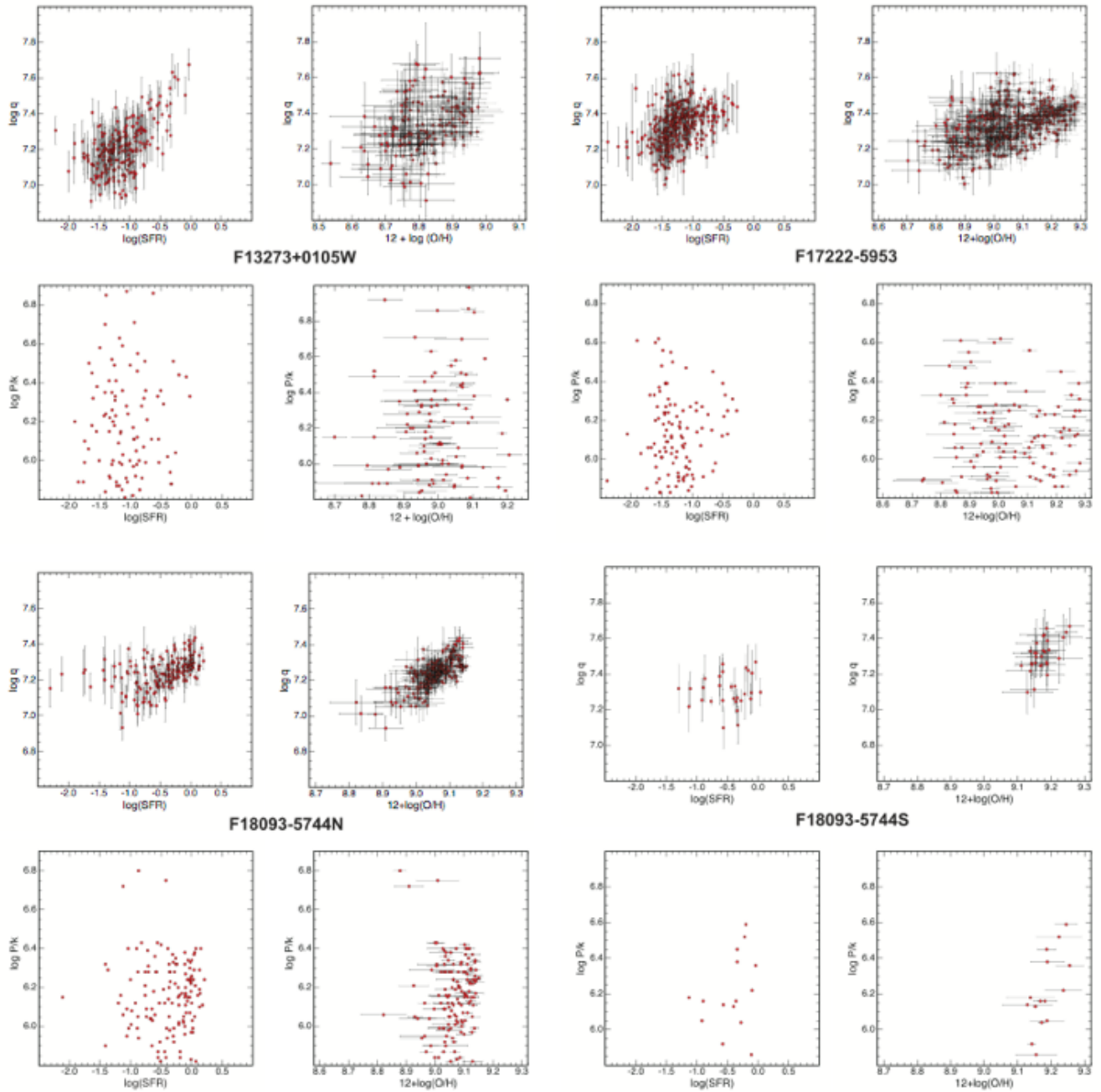


Fig. 11 As figure 9 but for F13273+0105W, F17222-5953 (ESO 138-G027), F18093-5744N (IC 4687) and F18093-5744S (IC 4689).

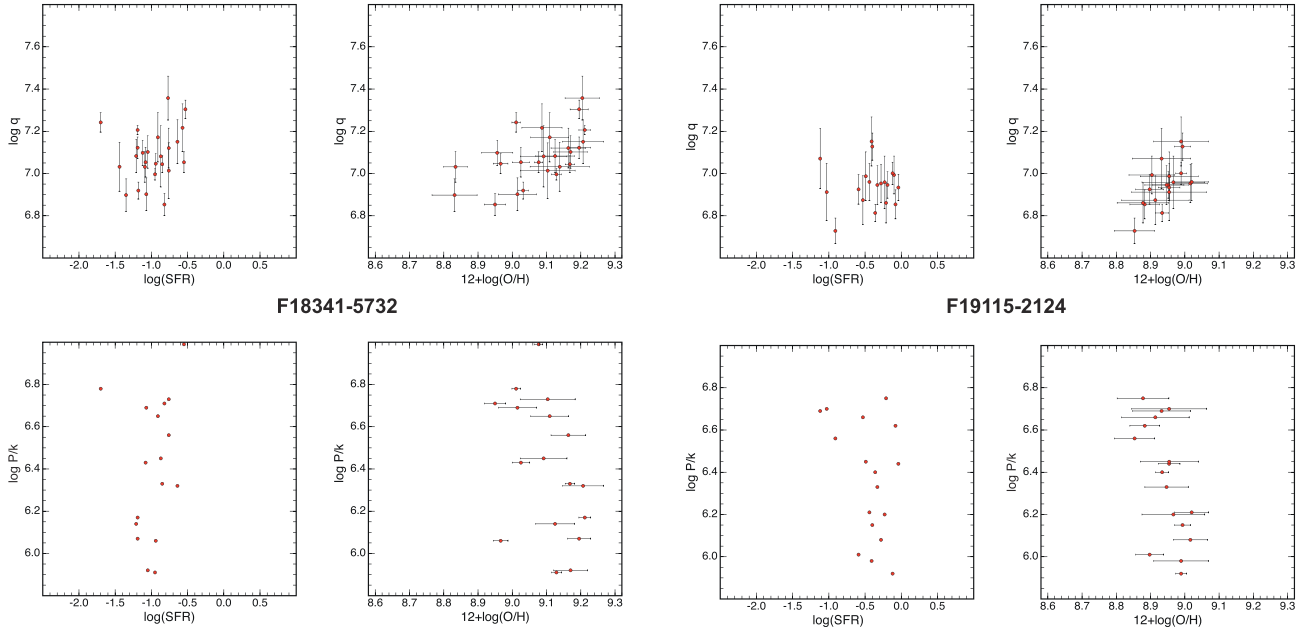


Fig. 12 As figure 9 but for F18341-5732 (IC 4734) and for F19115-2124 (ESO 593-IG008).

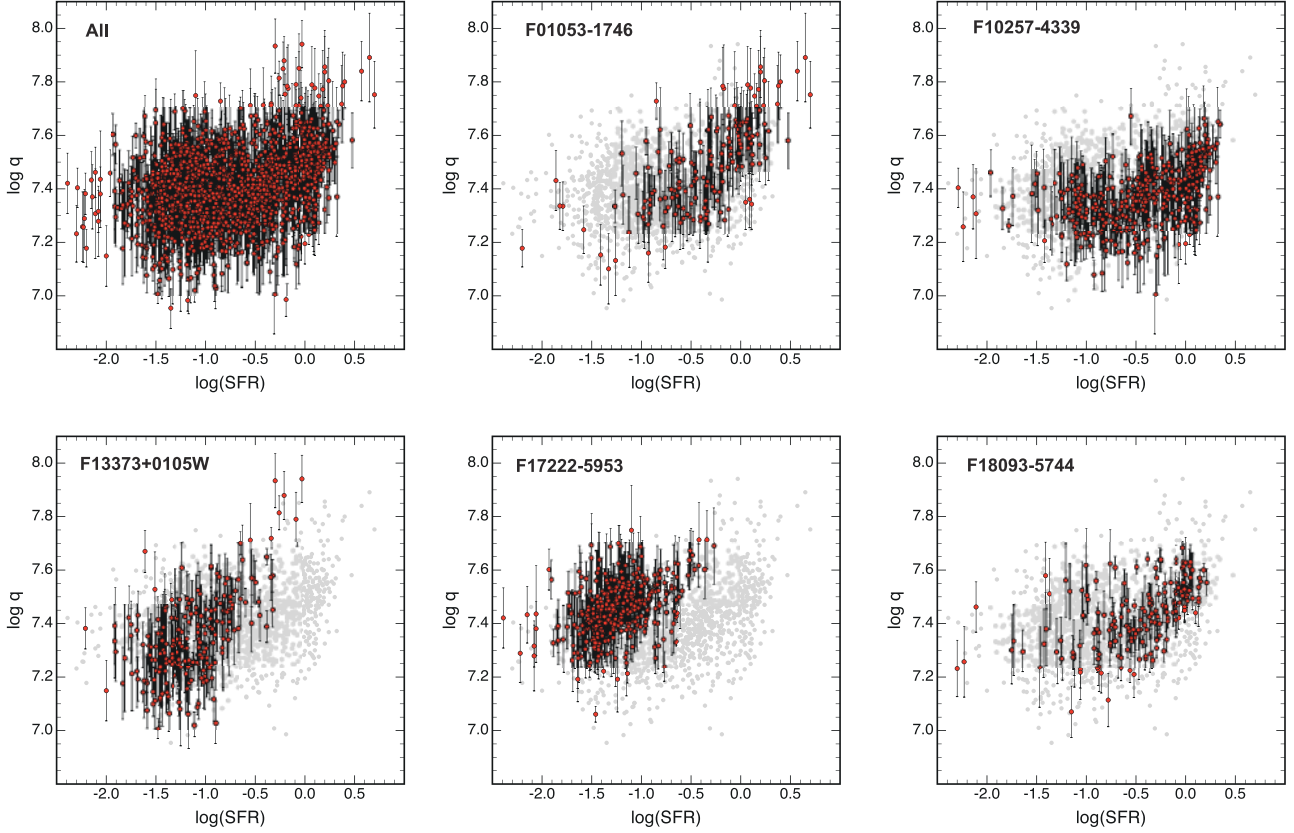


Fig. 13 Global $\log(\text{SFR})$ vs. $\log q$ correlations corrected for the local pressure. The ensemble of the points for all six galaxies are plotted in pale grey on the background. Above some threshold of star formation rate, which seems to vary galaxy to galaxy, all galaxies display correlation with a positive slope averaging at $q \propto \text{SFR}^{0.34}$.